Floor Identification in Large-Scale Environments with Wi-Fi Autonomous Block Models

Abstract—Traditional Wi-Fi based floor identification methods mainly have been tested in small experimental scenarios and, generally, their accuracies drop significantly when applied in real large and multi-storey environments. The main challenge emerges when the complexity of Wi-Fi signals on the same floor exceeds the complexity between the floors along the vertical direction, leading to a reduced floor distinguishability. A second challenge regards the complexity of Wi-Fi features in environments with atrium, hollow areas, mezzanines, intermediate floors, and crowded signal channels. We propose an adaptive Wi-Fi based floor identification algorithm to achieve accurate floor identification also in these environments. Our algorithm, based on the Wi-Fi RSSI and spatial similarity, firstly identifies autonomous blocks parcelling the whole environment. Then, local floor identification is performed through the proposed Wi-Fi models to fully harness the Wi-Fi features. Finally, floors are estimated through the joint optimization of the autonomous blocks and the local floor models. We have conducted extensive experiments in three real large and multi-storey buildings greater than 140,000 m2 using nineteen different devices. Finally, we show a comparison between our proposal and other state-of-the-art algorithms. Experimental results confirm that our proposal performs better than other methods and it exhibits an average accuracy of 97.24%.

Index Terms—floor identification, Wi-Fi model, fingerprint, smartphone, autonomous block, multi-storey buildings.

I. INTRODUCTION

INDOOR location-based services (ILBS) with smartphones have received increasing attention due to the high demand for location-aware applications [1][2]. In order to satisfy ILBS requirements, researchers have investigated several indoor positioning technologies, including Wi-Fi [3][4], Bluetooth Low Energy (BLE) [5], Pedestrian Dead Reckoning (PDR) [6],[7], vision camera based [8], and magnetic field [9][10][11]. These technologies applied in user localization, have shown good accuracies in 2D planes but their results are worse in 3D environments, especially in wide and multi-storey buildings.

In these environments, correct floor identification is a fundamental primary goal to effectively deploy an ILBS. Solutions based on a combination of Wi-Fi and barometer information have been widely investigated. In fact, information about the atmospheric pressure, theoretically, can be exploited as reliable discriminators to identify different floors. Unfortunately, the absolute value is difficult to be precisely measured with cheap barometers thus the air pressure is usually used to estimate relative floor changes. As an example, in HYFI [12], the authors updated the reference pressure of a floor with the Wi-Fi floor classification and evaluated short-term floor changes through air pressure information. However, the majority of commercial smartphones are not equipped with barometers and, therefore, Wi-Fi is still the most important information to develop floor identification methods. Consequently, Wi-Fi based methods are generally modelled as classification problems, including linear discriminant analysis (LDA) [13], k-means clustering [14], and deep neural network [15]. In

literature, several works rely on labelling the Wi-Fi fingerprints with the floor number where the readings have been collected and, then, by leveraging appearances of access points (APs) in fingerprints to mark the features as significant for the floors [12]. In those cases, the working hypothesis is considering the Received Signal Strength Indicator (RSSI) from an AP gathered at one floor stronger than the RSSI received from the same AP on other floors due, for example, to the attenuation introduced by walls. However, in wide and multi-storey buildings, the attenuation effect along horizontal direction becomes as obvious as the effect on different floors due to the presence of walls, rooms, people, and furniture which contribute to propagation loss. For each APs, the RSSI becomes weak at different floors but also at faraway places of the same floor. Although many Wi-Fi based methods have been presented, challenges for precise floor identification in complicated multi-storey environments are still open.

The first main challenge arises when the complexity of the environment on the same floor is comparable to the complexity along different floors. HYFI [12] leveraged probabilities of AP appearances in the whole floor as features. This system needs much time to collect enough samples and to ensure a correct balance across the floor. The slow convergence is a limitation and a drawback of the system. HyRise [16] only utilized the strongest signal strength to shrink the feature coverage, but the system also discards many information that could potentially improve the positioning performance. In order to tackle this problem, we propose to classify the building into multiple 3D autonomous blocks through a clustering algorithm based on Wi-Fi fingerprint using RSSI and spatial similarity. We define an autonomous block as a small spatial cell that contains similar RSSI and spatial features. Considering an autonomous block, the Wi-Fi fingerprints have reworked RSSI features thus decreasing the effect of the complexity on the same floor, and, successively, fine-grained Wi-Fi models are used to improve floor identification performance for each autonomous block.

A second challenge regards the handling of Wi-Fi failures in complex environments, which include open spaces, mezzanines and intermediate floors, large and multi-storey areas, and crowded signal channels. A failure during a Wi-Fi scan might also be caused by too weak signals from a faraway AP or by channel interferences due to crowded signal channels. Existing works [17],[13] suggest to fill failed AP scans with the minimum detectable RSSI value, for example $-90dBm$. However, if the failure is caused by channel interference, the minimum value will wrongly indicate that the signal is coming from a remote AP. Considering the Wi-Fi characteristic in complex scenarios, we propose a fine-grained Wi-Fi model to discern them and fully utilize the available Wi-Fi features. Then, we estimate different floors through the joint optimization of autonomous block detection and local floor identification. We have performed several experiments in real-world scenarios, and we claim that the proposed algorithm improves the floor

identification accuracy in complex environments.

Specifically, we provide the following contributions:

• Augmented K-means clustering algorithm, based on Wi-Fi RSSI and spatial similarity, to overcome the complexity on the same floor.

• Enhanced Bayesian Wi-Fi models for fine-grained indoor positioning able to fully utilize all the available information from a Wi-Fi scan. Our algorithm automatically identifies several autonomous blocks inside the whole environment and then it optimizes the floor identification.

• We have conducted extensive experiments to test our algorithm in 3 real-world buildings. The deployment area is greater than $140,000m^2$. Results reveal that the proposed algorithm achieves high accuracies and robust performances as compared with state-of-the-art methods.

The rest of the paper is organized as follows. Related works are reviewed in section II. Section III describes Wi-Fi fingerprints and provides a system overview. Section IV introduces the autonomous block clustering algorithm. section V shows the proposed fine-grained Wi-Fi model and our floor identification methods. Implementation details and experimental results are presented and discussed in section VI. Finally, Section VII concludes this paper and analyses future works.

II. RELATED WORK

A. Wi-Fi based Floor Identification

Wi-Fi based floor identification has been usually approached considering Wi-Fi fingerprints collected at the same floor similar and grouped together. A supervised learning model has been used to identify the right floor. Luo et al. [13] proposed the linear discriminant analysis (LDA) to build a multi-floor Wi-Fi fingerprint database. They leveraged a majority voting mechanism to identify the floor. Their work solved the high computation complexity problem existing in several works containing a similar approach. Kim et al. [15] analysed the hierarchical and different nature of the building/floor/location estimation and designed a single-input and multi-output deep neural network (DNN) to enable the hybrid regression. However, these works ignored the inherent complexity of radio-wave propagation in indoor environments. ViFi [18] proposed a Wi-Fi RSSI prediction method based on a multi-wall and multi-floor (MWMF) propagation model to generate a discrete RSSI radio map, which allowed a sevenfold reduction in the number of measurements to be collected. The inherent complexity of Wi-Fi propagation in indoor environments increases the risk of identifying a sequence of floors at different levels, so introducing a sequence of vertical jumps of the final position estimation. Consequently, researchers have attempted to refine the vertical motion detection in order to perform floor identification updating the estimation only when vertical motions have been detected.

B. Integrated Floor Identification

Generally, acceleration and pressure information are used to detect vertical motions. HyRise [16] modelled the pressure with a finite state machine, then it updated the Wi-Fi probabilities of each floor according to the pressure states.

TABLE I
A COMPARISON BETWEEN FLOOR IDENTIFICATION ALGORITHM

Ref	Method	Wi-Fi	Pressure	IMU
[13]	Linear discriminant analysis	✓		
[15]	Deep neural network	✓		
[18]	Multi-wall and multi-floor model	✓		✓
[16]	Markovian probability	✓	✓	
[19]	HORUS algorithm	✓	✓	✓
[12]	Bayesian Classification	✓	✓	
[20]	Indoor outdoor detection + WKNN	✓	✓	

Banerjee et al. [19] leveraged pressure values to adjust floor change probabilities in their Wi-Fi based algorithms. The authors also leveraged stationary detection to eliminate the barometer drift problem. Since the atmospheric pressure decreases when the altitude increases, researchers have proposed several barometer-based floor identification solutions. In order to estimate the absolute floor number, a reference barometer station is necessary: HYFI [12] utilized Wi-Fi positioning results as virtual reference stations; Bisio et al. [20] proposed an indoor/outdoor (I/O) detection to determine the first-floor pressure as the virtual reference station. However, barometers are only equipped in few models of smartphones, thus limiting the real application of pressure based methods.

As TABLE I reveals, although the accelerometer/gyroscope/pressure patterns have been used to improve the performance of floor identification, based on the analysis of existing works, we can conclude that Wi-Fi is still the most important and common signal for enabling a ubiquitous floor identification. Seldom the works in literature have fully considered also the issues encountered in real large-scale multi-storey environments, including the problem of an increased signal heterogeneity on the same floor, and a strong channel interference. Our work analyses the two issues and proposes the clustering method to identify autonomous blocks and Wi-Fi models to implement robust and accurate floor identification.

III. SYSTEM OVERVIEW

In this section we first describe the working principles of Wi-Fi fingerprint and, successively, we describe the system overview.

A. Working principles of Wi-Fi Fingerprints

As shown in Fig. 1, our system consists of two phases: an offline-phase to train a floor model and an online phase to detect floors based on the model. In the off-line phase, a site-surveyor walk around the building holding one smartphone to periodically collect Wi-Fi fingerprints and fingerprint coordinates of all reachable areas at different floors (inputted by the same site-surveyor). The combination of a Wi-Fi fingerprint and its coordinates is called a sample. Samples of the whole building are sent to a training server, then are processed to get a floor detection model. Considering the discernibility of Wi-Fi signals, the distance between two samples is less than two meters, comparable to the positioning accuracy of RSSI based positioning systems [21]. On the other hand, it is suggested to collect fingerprints at the working time so assuring

TABLE II
NAMING CONVENTION OF VARIABLES, SUPERSCRIPTS, AND SUBSCRIPTS

| Item	Description
Superscript (e.g., N^S, N^A)	To discriminate variables of different types. E.g., N^S, N^A, N^B represent the total number (N) of samples (S), APs (A), and autonomous blocks (B).
Subscript (e.g., $r_{h,i}$)	To represent data indexes. h, i, j, k are indexes of samples, APs, floors, and autonomous blocks. E.g., $r_{h,i}$ is the RSSI (r) of AP_i observed in sample s_h.
Script character (e.g., $\mathcal{NF}^B, \mathcal{NF}^F$)	To represent the events after a Wi-Fi scan in the autonomous block and local floor detections. E.g., $\mathcal{NF}^B$ is the event "negative AP and false scan" $\mathcal{NF}$ for an autonomous block (B). $\mathcal{NF}^F$ is the event "negative AP and false scan" ($\mathcal{NF}$) for the local floor (F).
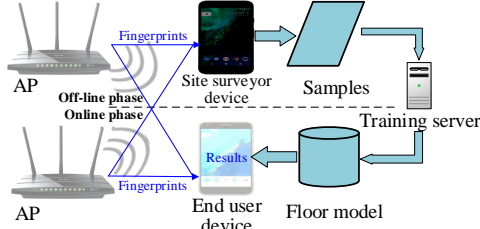
Fig. 1. The data flow of off-line and online phases.

realistic features of collected fingerprints in accordance with the supposed use of the system.

In the online phase, end-users download the floor detection model form the training server using a dedicated smartphone app. The smartphone collects real-time Wi-Fi fingerprints and, based on the model, estimates the floor where the user is.

For clarity, the naming convention of variables used in this paper is summarized in TABLE II. The representations of fingerprint coordinates and fingerprints are as follows. As shown in equation (1), according to TABLE 2, the system utilizes loc_h, a triple of real numbers, to represent the fingerprint coordinates. Variable z contains the number of the floor. N^S is the total number of samples collected into the building. The maximum Wi-Fi sampling frequency is around 0.5Hz thus the time used for sampling is approximated to 2 seconds. When the average sample density is greater than $1\ sample/m^2$, the proposed system reaches a stable floor identification accuracy. Accordingly, the sampling time is around two times the building area in square meters. Equation (2) reveals the structure of a Wi-Fi fingerprint fp_h, a list of observed MAC and RSSI pairs at location loc_h. The total number of APs is N^A. In equation (3), $r_{h,i}$ depicts the RSSI of a smartphone scanning AP_i at location loc_h. If an AP is successfully scanned, the smartphone collects the RSSI as a negative integer. Otherwise, we set the RSSI value with $Null$. Samples collected during the off-line phase can be represented in equation (4). A sample s_h is a couple of location loc_h and the observed Wi-Fi fingerprint fp_h. During the online phase, the user position is unknown and, therefore, we utilize fp and r_i to represent online fingerprint and RSSI.

$$loc_h \in \{(x_h, y_h, z_h)|x_h, y_h, z_h \in \mathbb{R}\}, h \in [1, N^S] \quad (1)$$

$$fp_h = \{\langle MAC_{h,i}, r_{h,i}\rangle i \in [1, N^A]\}, h \in [1, N^S] \quad (2)$$

$$r_{h,i} \in \{\mathbb{N}^- \cup \{Null\}\}, h \in [1, N^S], i \in [1, N^A] \quad (3)$$

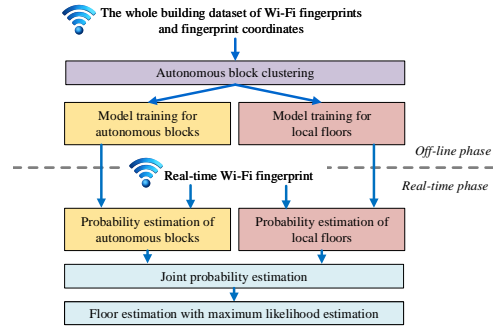$$s_h = \langle loc_h, fp_h\rangle, h \in [1, N^S] \quad (4)$$

Fig. 2. Overview of the proposed system.

B. System Architecture

The proposed system architecture, shown in Fig. 2, relies on seven functional modules: (a) autonomous block clustering, (b) model training for autonomous blocks, (c) model training for local floors, (d) probability estimation of autonomous blocks, (e) local floor probability estimation, (f) joint probability estimation, and (g) floor estimation with maximum likelihood estimation (MLE).

(a) Autonomous block clustering: the module clusters the training Wi-Fi dataset of a building into several autonomous blocks, within which the Wi-Fi fingerprints have similar RSSI and spatial features.

(b) Model training for autonomous block: based on the clustered Wi-Fi fingerprints, the module performs the model training for autonomous block detection by evaluating the statistical features of each autonomous block.

(c) Model training for local floor identification: for each autonomous block, based on the floor number of the Wi-Fi dataset, the module performs the model training for the local floor identification by evaluating the statistical features of each floor.

(d) Probability estimation of autonomous block: in the online phase, when a real-time Wi-Fi fingerprint is collected, the module calculates the probabilities of the fingerprint for each autonomous block.

(e) Probability estimation of local floor: the module calculates the probabilities of the received fingerprint for every floor in every autonomous block.

(f) Joint probability estimation: the module calculates the joint probability of all the combinations of autonomous blocks and their local floors, given the received fingerprint.

(g) Floor estimation with MLE: the module estimates the final floor number of the real-time Wi-Fi fingerprint by selecting the floor number with the maximum likelihood probability of all the joint probabilities.

IV. AUTONOMOUS BLOCK CLUSTERING WITH RSSI AND SPATIAL SIMILARITY

The basic principle of Wi-Fi based floor identification is to consider the APs signal variation at different floors. However, as the size of the building enlarges, AP signals are also attenuated by walls and propagation loss along the horizontal direction. Therefore, when the building size is large enough, the Wi-Fi signal heterogeneity along the horizontal direction is even wider than the heterogeneity along different floors. This
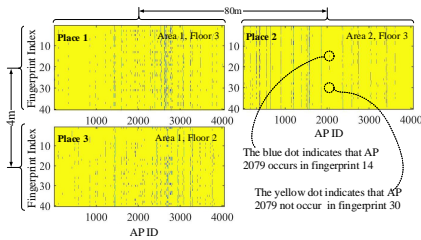
Fig. 3. Wi-Fi fingerprint comparison of different floors and areas.
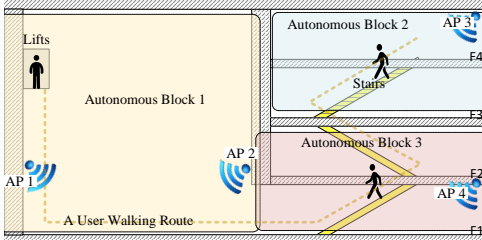

Fig. 4. Clustering autonomous block through Wi-Fi fingerprint.

phenomenon leads to inaccuracies. For example, Fig. 3 shows a comparison between Wi-Fi fingerprints collected in three different areas, $100m^2$ large, of the same building. Place 1 and 2 belong to the same floor. Place 1 and 3 belong to different floors and place 3 is below place 1 of 4 meters. The total number of APs observed in the building is 4058. We collected 40 Wi-Fi fingerprints in each of the three places. The figure shows a comparison of the fingerprints collected based on the presence of APs. If an AP occurs in a fingerprint, the AP is represented as a blue pixel, otherwise as a yellow pixel. Pixels of the same row represent the occurrences of APs in a Wi-Fi fingerprint. Pixels of the same column show occurrences of an AP in different fingerprints. In the example shown, the fingerprints heterogeneity increases from floor 3 to floor 2 in the same area 1 thus they can be used to discriminate floors in the area 1. Unfortunately, the Wi-Fi heterogeneity between place 1 and place 2 on the same floor 3 is even greater than the previous (i.e., the correlation coefficient between Area 1 and 2 is -0.03 and the coefficient between Area 1 and 3 is 0.18). In fact, the spatial distance between place 1 and place 2 is about 80 meters and, due to the many obstacles in the middle, we observe strong Wi-Fi signals attenuation. This problem is common in large and multi-storey buildings and, therefore, indoor positioning systems reach low performances in floor identification.

To address this problem, we propose to divide the environment into several autonomous blocks with clustering techniques. Inside each autonomous block, Wi-Fi fingerprints have similar features both in RSSI and spatial spaces. Then, we can construct local floor identification models for each autonomous block thus reducing the interferences on the same floor.

Fig. 4 shows a graphic representation of our autonomous block clustering. Four APs are deployed on different floors of a building. Considering the weak penetration of Wi-Fi signals, the building can be divided into three autonomous blocks based on observable APs.

Floors and walls divide the whole building into several blocks, thus APs in the same autonomous block have two
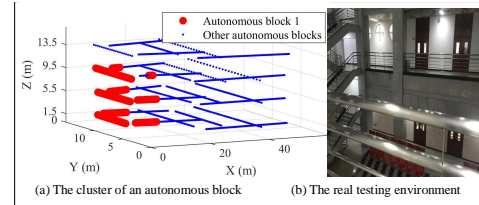

Fig. 5. An example of an autonomous block clustering.

features: they are close to each other and only few obstacles are in the middle. Therefore, also the fingerprints collected into the same block are similar to each other. In other words, as Fig. 3 reveals, place 2 is more different to place 1 than place 3, but these differences are irrelevant for floor detection. Our system clusters place 1 and 2 into two different autonomous blocks to isolate the differences of fingerprints on the same floor.

Fig. 5 shows an example in which one dot corresponds to a location on which a Wi-Fi fingerprint has been collected. Based on these samples, our system performs clustering to create autonomous blocks. The red dots in Fig. 5(a) belong to the same autonomous block, the blue dots belong to other blocks. As stated before, our algorithm clusters Wi-Fi fingerprints with similar signal similarity and spatial proximity into the same autonomous block which generally covers multiple floors. Also, fingerprints collected at lobbies, hallways, and mezzanines are clustered into the same autonomous block. Therefore, we apply a local fine-grained Wi-Fi model to refine and improve the floor detection performances.

Wi-Fi fingerprint samples gathered into a multi-storey environment compose a large dataset. Therefore, we propose the efficient K-means method [22], shown in Algorithm I, as the clustering algorithm for the autonomous block identification. The input D is the whole building dataset of Wi-Fi fingerprints and fingerprint coordinates $D = \{s_h | h \in [1, N^S]\}$. N^B is the target number of the autonomous blocks. The algorithm clusters Wi-Fi fingerprints and produce N^B autonomous blocks with the related fingerprint sets. When the algorithm starts, the centroids of each autonomous block are randomly initialized. Then, it analyses all the instances s_h and evaluates the distance $d_{h,k}$ from s_h to all centroids. Successively, the autonomous block membership $memb_h$ of s_h is classified as the centroid $ctr_k (1 \le k \le N^B)$ with the minimum distance.

As equation (5) reveals, the centroid ctr_k of an autonomous block consists of two parts: fingerprint centroid $fctr_k$ and spatial centroid $sctr_k$. The form of $fctr_k$ and $sctr_k$ are equals to fp_h and loc_h respectively.

$$ctr_k = \langle fctr_k, sctr_k \rangle, k \in [1, N^B] \qquad (5)$$

Accordingly, our algorithm leverages the Jaccard [23] and Euclidean distance to measure the similarity and proximity of Wi-Fi fingerprints. As Fig. 4 reveals, considering the weak penetration of Wi-Fi signals, the RSSI of AP 1 is undetectable in autonomous block 2 because the signal becomes too weak. In other words, the RSSI of an AP is only detectable in a small area of a large building. Therefore, our system leverages the similarity of detectable AP set as a gauge for clustering. As equation (6) reveals, the detectable AP set is the MAC part of the equation (2).

$$fm_h = \{MAC_{h,i} | i \in [1, N^A]\}, h \in [1, N^S] \qquad (6)$$

Algorithm 1 The autonomous block clustering algorithm

Require: D, N^B

1: Initilize autonomous block centroids ctr_k randomly
2: **repeat**
3:     **for each** $s_h \in D$ **do**
4:        Init shortest distance $sd_h \leftarrow MaxDistance$
5:        Init membership $memb_h \leftarrow null$
6:        **for each** ctr_k **do**
7:           $d_{h,k} \leftarrow$ calculate distance from s_h to c_k
8:           **if** $d_{h,k} < sd_h$ **then**
9:              $sd_h \leftarrow d_{h,k}$
10:             $memb_h \leftarrow ctr_k$
11:           **end if**
12:        **end for**
13:     **end for**
14:     Update autonomous block fingerprint centroid $fctr_k$
15:     Update autonomous block spatial centroid $sctr_k$
16: **until** Converge

Specifically, we utilize the normalized Jaccard distance $jdis_{h,k}$ to measure the similarity of detectable AP sets. It is defined as the size of the intersection divided by the size of the union of the sample sets. As equation (7) reveals, $fctr_k$ is the Wi-Fi fingerprint of the centroid ctr_k. $|fm_h \cap fctr_k|$ is the number of common occurrences of AP MACs in two Wi-Fi fingerprints. The factor is normalized by the possible maximum number of $|fm_h \cap fctr_k|$. Basically, fingerprint samples with the greatest number of common APs are clustered into the same autonomous block.

$$jdis_{h,k} = 1 - \frac{|fm_h \cap fctr_k|}{\max\limits_{1 \leq u1 \leq N^S, 1 \leq u2 \leq N^B} |fm_{u1} \cap fctr_{u2}|}, \quad (7)$$
$$h \in [1, N^S], k \in [1, N^B]$$

APs within the same autonomous block are also physically close to each other, thus we utilize the Euclidean distance $edis_{h,k}$ to measure the proximity between fingerprints in the spatial domain. As equation (8) reveals, $sctr_k$ is the coordinates of the centroid ctr_k. The factor is normalized by the possible maximum spatial distance of $\| loc_h - sctr_k \|_2$.

$$edis_{h,k} = \frac{\| loc_h - sctr_k \|_2}{\max\limits_{1 \leq u1 \leq N^S, 1 \leq u2 \leq N^B} \| loc_{u1} - sctr_{u2} \|_2}, \quad (8)$$
$$h \in [1, N^S], k \in [1, N^B]$$

Jaccard and Euclidean distances are two important factors that influence the performance of autonomous block clustering and floor identification. The distance $d_{h,k}$ from the sample s_h to the centroid ctr_k is a combination of the Jaccard and Euclidean distances, as shown in equation (9). Considering the complexity of indoor environments, the proportion α of the two distances should be determined empirically.

$$d_{h,k} = \alpha \cdot jdis_{h,k} + (1 - \alpha) \cdot edis_{h,k}, \quad (9)$$
$$h \in [1, N^S], k \in [1, N^B]$$

When an iteration ends, the centroids of each autonomous block are recalculated. As equation (10) shows, the RSSI centroid $fctr_k$ is the union of all the AP MACs classified as the centroid. The union operation guarantees that Wi-Fi fingerprints that have more common MACs are classified as the same autonomous block.

$$fctr_k = \underset{memb_u == ctr_k}{union}(F_u), k \in [1, N^B] \quad (10)$$
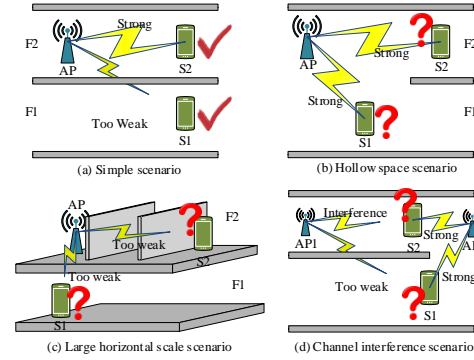

Fig. 6. Wi-Fi features in different indoor scenarios.

The spatial centroid $sctr_k$ shown in equation (11) is the average coordinates of all the fingerprints that belong to the same autonomous block. In the training phase, the algorithm iterates until the centroids of autonomous blocks converge so training samples are clustered into autonomous blocks.

$$sctr_k = \frac{\underset{memb_u == ctr_k}{vectorSum(loc_u)}}{count(memb_u == ctr_k)}, k \in [1, N^B] \quad (11)$$

Possible autonomous blocks range from 1 to N^S. In order to find the optimal value, we leverage the elbow method [24]—an effective way to find the right K in K-means based clustering—to determine the value of N^B. As equation (12) reveals, the distortion of the resulting cluster is the sum of the squared distance between a sample and its centroid. A lower distortion means that the samples within a cluster are closer to each other. The basic idea of the elbow method is that the distortion decreases as the number of clusters increases. It first decreases fast then slowly after a critical K value. The critical K value is the elbow point and, in our algorithm, it represents the right number of autonomous blocks.

$$distortion = \sum_{h=1}^{N^S} (d_{h,memb_h})^2 \quad (12)$$

V. WI-FI MODEL AND ACCURATE FLOOR IDENTIFICATION

As previously discussed, Wi-Fi signals are affected by many factors, including obstacles, building structures, channel interferences, and propagation loss. For example, Fig. 6(a) shows a simple scenario in which AP signals are attenuated by floors and, therefore, a floor can be identified through the AP detection. Generally, in large and multi-storey buildings, raised or intermediate floors, and mezzanines are often present. In Fig. 6(b), no floor causes an AP signal attenuation on floor 2. Then, the signal is still strong at F1 and F2, decreasing the floor distinguishability. On the contrary, in Fig. 6(c), when a smartphone is too far from an AP, the AP signal is attenuated by walls along the horizontal direction, making it weak on the same floor and other floors. When more APs are deployed, it is worth noting that the AP channel number is limited, so the risk of channel interference increases. In Fig. 6(d), smartphone S2 may fail to correctly scan AP1 due to channel interference introduced from AP2. In this situation, the Wi-Fi information may appear as retrieved on F1.

Fig. 7. shows a summary of the scenarios discussed in Fig.5. Basically, only when a smartphone successfully scans
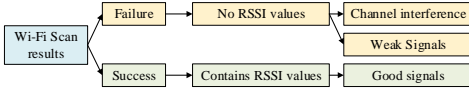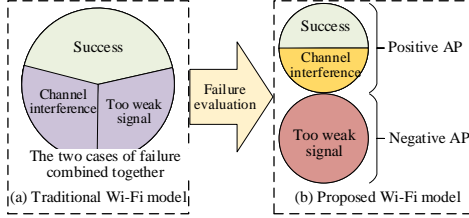
Fig. 7. Potential Wi-Fi scan results.

Fig. 8. Wi-Fi model comparison.

an AP it detects the RSSI of the AP. The RSSI value can be used to depict the smartphone's proximity to the AP. A failed Wi-Fi scan might be caused by a too weak signal or due to channel interference. A failure due to too weak signal suggests that a user is far away from the AP. Instead, a failure due to channel interference may occur also when a user is close to the AP. Unfortunately, the failure due to channel interference is less easily recognizable. Traditional Wi-Fi based floor identification methods generally ignore the reasons of scan failures, therefore limiting the performances.

A. Probability Estimation of an Autonomous Block

In order to accurately identify floors in complex scenarios, it is necessary to precisely model the features of Wi-Fi scans. Considering a real-time Wi-Fi fingerprint, no information is available to directly discern the reasons of a Wi-Fi scan failure. We propose to identify failures for too weak signals by labelling out far away APs in the training phase. Specifically, the space of the whole building is divided into several small cells based on the clustered autonomous blocks. In other words, a cell is a small portion of the building which has similar RSSI features. We classify the APs into two types: positive and negative. For each cell, positive APs are the ones that appeared at least once in the cell, corresponding to success or interference case in Fig. 8 (b). Negative APs are the ones that never appeared in the cell considered but appeared in other cells, corresponding to the too weak signal case. Then, considering a failed Wi-Fi scan in a real-time Wi-Fi fingerprint, if the AP is marked as negative in a cell, the failure is considered as a failure due to a too weak signal for the cell. On the other hand, if the AP is positive, then the failure is considered a failure due to channel interference.

The paper proposes a hierarchical probability model to represent the Wi-Fi fingerprints feature of a block. Based on the order of magnitudes, the probabilities can be classified into three level of granularity. The high granularity is related to faraway APs. The middle granularity is related to the appearance of the AP into the block. The low granularity is related to received signal strength from an AP of the block. TABLE 3 shows detail of the enhanced Bayesian Wi-Fi model for autonomous block detection proposed in this paper. For the real-time phase, when a new Wi-Fi fingerprint is available, we classify the APs into the fingerprint as true or false. True APs are the ones that have been detected in the fingerprint and have

TABLE III
WI-FI MODEL FOR AUTONOMOUS BLOCK DETECTION

Autonomous block model		AP results in online fingerprint	
		True scan ($\mathcal{T}$)	False scan ($\mathcal{F}$)
Off-line autonomous block model	Positive AP ($\mathcal{P}$)	$P(r_i, S_{i,k}^B)$	$P(F_{i,k}^B)$
	Negative AP ($\mathcal{N}$)	$P(\mathcal{NT}^B) \equiv 0$	$P(\mathcal{NF}^B) \equiv 1$

appeared in the off-line phase. False APs are the ones that have appeared in the off-line phase, but they have not been detected in the new fingerprint. The joint probability of a positive AP and a true scan ($\mathcal{PT}$) result is $P(r_i, S_{i,k}^B)$, $S_{i,k}^B$ is the event of successful detecting the i_{th} AP in the k_{th} autonomous block. As equation (13) reveals, $P(r_i, S_{i,k}^B)$ equals to the product of $P(r_i|S_{i,k}^B)$ and $P(S_{i,k}^B)$. $P(r_i|S_{i,k}^B)$ is modelled as Gaussian distribution. $\mu_{i,k}^B$ and $\sigma_{i,k}^B$ are the RSSI mean and variance of the i_{th} AP in the k_{th} autonomous block. $P(S_{i,k}^B)$ is the scan success probability.

$$\begin{cases} P(r_i, \mathcal{S}_{i,k}^B) = P(r_i|\mathcal{S}_{i,k}^B)P(\mathcal{S}_{i,k}^B) \\ P(r_i|\mathcal{S}_{i,k}^B) = N(\mu_{i,k}^B, \sigma_{i,k}^B) \\ P(\mathcal{S}_{i,k}^B) = \frac{SuccessfulScanNumber}{TotalScanNumber} \end{cases} \quad (13)$$

As equation (14) reveals, $P_k^B(\mathcal{F}_{i,k}^B)$ is the probability of a positive AP and a false scan ($\mathcal{PF}$). In other words, the probability of a failure in detecting the not far i_{th} AP. The probability reflects the channel interference level.

$$P(\mathcal{F}_{i,k}^B) = 1 - P(\mathcal{S}_{i,k}^B) \quad (14)$$

The probability of a negative AP and a true scan ($\mathcal{NT}$) result $P(\mathcal{NT}^B)$ is constant to zero, indicating that an AP is far away from an autonomous block and, if the AP is detected, then the user should not be in the autonomous block. However, considering that the sample time is limited, for a real application, we replace the zero with a small probability value. The probability of a negative AP and false scan ($\mathcal{NF}$) result $P(\mathcal{NF}^B)$ is constant to one.

In the offline phase, the system calculates $P(S_{i,k}^B)$, $\mu_{i,k}^B$ and $\sigma_{i,k}^B$ for all AP in every autonomous block to get the autonomous block detection model. Then, based on the model, in the online phase, given a real-time Wi-Fi fingerprint fp and an autonomous block B_k, the probability $P(B_k|fp)$—fp lies in B_k—can be calculated. Based on TABLE 3, all the r_i of fp can be classified into four sets: $set_k^{\mathcal{PT}}$, $set_k^{\mathcal{PF}}$, $set_k^{\mathcal{NT}}$ and $set_k^{\mathcal{NF}}$, corresponding to the $\mathcal{PT}$, $\mathcal{PF}$, $\mathcal{NT}$ and $\mathcal{NF}$ events that occur during the online phase.

Based on the Bayesian rule, given the initial probabilities of every autonomous block are equal, then $P(B_k|fp)$ is proportional to $P(fp|B_k)$ which is the probability of observing the fp in block B_k, shown in equation (15).

$$P(B_k|fp) = \frac{P(fp|B_k)P(B_k)}{\sum_{l=1}^{N^c} P(fp|B_k)P(B_k)} \propto P(fp|B_k) \quad (15)$$

Considering that APs are independent of each other, therefore, as equation (16) reveals, $P(fp|B_k)$ is the joint probability of every r_i in the block B_k.

$$P(fp|B_k) = \prod_{r_i \in set_k^{\mathcal{PT}}} P(r_i, \mathcal{S}_{i,k}^B)$$

$$\prod_{r_i \in set_k^{\mathcal{PF}}} P(\mathcal{F}_{i,k}^B) \prod_{r_i \in set_k^{\mathcal{NT}}} P(\mathcal{NT}^B) \prod_{r_i \in set_k^{\mathcal{NF}}} P(\mathcal{NF}^B) \quad (16)$$

Taking the equation (16) into (15) and considering the $P(\mathcal{NF}^B)$ constantly equals one, then the probability of an

TABLE IV
WI-FI MODEL FOR FLOOR IDENTIFICATION

Floor model		AP results in online fingerprint	
		True scan ($\mathcal{T}$)	False scan ($\mathcal{F}$)
Off-line floor model	Positive AP ($\mathcal{P}$)	$P(r_i, S_{i,j,k}^F)$	$P(\mathcal{F}_{i,j,k}^F)$
	Negative AP ($\mathcal{N}$)	$P(\mathcal{N}\mathcal{T}^F) \equiv 0$	$P(\mathcal{N}\mathcal{F}^F) \equiv 1$

autonomous block B_k given an online fingerprint fp can be calculated with equation (17).

$$P(B_k|fp) \propto$$
$$\prod_{r_i \in set_k^{\mathcal{P}\mathcal{T}}} P(r_i, \mathcal{S}_{i,k}^B) \prod_{r_i \in set_k^{\mathcal{P}\mathcal{F}}} P(\mathcal{F}_{i,k}^B) \prod_{r_i \in set_k^{\mathcal{N}\mathcal{T}}} P(\mathcal{N}\mathcal{T}^B) \quad (17)$$

After normalization, we can conclude the equation (18), the final form of autonomous block probability estimation.

$$P(B_k|fp) =$$
$$\frac{\prod_{r_i \in set_k^{\mathcal{P}\mathcal{T}}} P(r_i, \mathcal{S}_{i,k}^B) \prod_{r_i \in set_k^{\mathcal{P}\mathcal{F}}} P(\mathcal{F}_{i,k}^B) \prod_{r_i \in set_k^{\mathcal{N}\mathcal{T}}} P(\mathcal{N}\mathcal{T}^B)}{\prod_{u \in set^B} \left(\prod_{r_i \in set_u^{\mathcal{P}\mathcal{T}}} P(r_i, S_{i,m}^B) \prod_{r_i \in set_u^{\mathcal{P}\mathcal{F}}} P(\mathcal{F}_{i,m}^B) \prod_{r_i \in set_u^{\mathcal{N}\mathcal{T}}} P(\mathcal{N}\mathcal{T}^B) \right)} \quad (18)$$

where set^B is the set of all the available autonomous blocks.

B. Probability Estimation of a Floor in an Autonomous Block

Evaluated the probabilities of the autonomous blocks, we construct a similar Wi-Fi model in order to estimate the floor probability into the blocks. Basically, we separate too weak signals and failures due to interferences with the granularity of the floor. For each floor, as shown in TABLE 4, APs in the training model of a floor have also been classified into positive and negative. The positive AP is the one that has appeared on the floor. Negative APs only appear on other floors of the autonomous block. In TABLE 4, the event $\mathcal{S}_{i,k,j}^F$ is a successful detection of the i_{th} AP in the k_{th} autonomous block at the j_{th} floor. The event $\mathcal{F}_{i,k,j}^F$ is a failed scan of a positive AP. The event $\mathcal{N}\mathcal{T}^F$ is a true scan of a negative AP. $\mathcal{N}\mathcal{F}^F$ is a false scan of a negative AP.

The model training of floor detection in an autonomous block is similar to the autonomous block detection model. The system calculates the probability of successful detecting the i_{th} AP in the k_{th} autonomous block at the j_{th} floor $P(\mathcal{S}_{i,k,j}^F)$, and corresponding mean $\mu_{i,k,j}^F$ and variable $\sigma_{i,k,j}^F$ Then, comparing to the equation (15), we can conclude that $P(F_j|fp, B_k)$ is the floor F_j probability in the autonomous block B_k, given an online scan result fp, shown in equation (19). Given that the prior probabilities of the user's location distributed on different floors of the autonomous block are equal, $P(F_j|B_k)$ is equal for each floor. The factor $P(fp|B_k)$ is a constant value for each floor. Therefore, $P(F_j|fp, B_k)$ is proportional to $P(fp|F_j, B_k)$, that is, the probability of observing the scan result fp at the F_j floor in the autonomous block B_k.

$$P(F_j|fp, B_k) = \frac{P(fp|F_j, B_k)P(F_j|B_k)P(B_k)}{P(fp|B_k)P(B_k)}$$
$$= \frac{P(fp|F_j, B_k)P(F_j|B_k)}{P(fp|B_k)} \propto P(fp|F_j, B_k) \quad (19)$$

Based on the AP independence, $P(fp|F_j, B_k)$ is the joint probability of every r_i appearing at the F_j floor in the block

B_k. Comparing to the equation (16) and (17), we can conclude that:

$$P(F_j|fp, B_k) \propto$$
$$\prod_{r_i \in set_{k,j}^{\mathcal{P}\mathcal{T}}} P(r_i, \mathcal{S}_{i,k,j}^F) \prod_{r_i \in set_{k,j}^{\mathcal{P}\mathcal{F}}} P(\mathcal{F}_{i,k,j}^F) \prod_{r_i \in set_{k,j}^{\mathcal{N}\mathcal{T}}} P(\mathcal{N}\mathcal{T}^F) \quad (20)$$

where $set_{k,j}^{\mathcal{P}\mathcal{T}}$, $set_{k,j}^{\mathcal{P}\mathcal{F}}$, $set_{k,j}^{\mathcal{N}\mathcal{T}}$ correspond to the $\mathcal{P}\mathcal{T}$, $\mathcal{P}\mathcal{F}$ and $\mathcal{N}\mathcal{T}$ AP set at the j_{th} floor in the k_{th} autonomous block. After normalization, we can write the equation (21),

$$P(F_j|fp, B_k) =$$
$$\frac{\prod_{r_i \in set_{k,j}^{\mathcal{P}\mathcal{T}}} P(r_i, \mathcal{S}_{i,k,j}^F) \prod_{r_i \in set_{k,j}^{\mathcal{P}\mathcal{F}}} P(\mathcal{F}_{i,k,j}^F) \prod_{r_i \in set_{k,j}^{\mathcal{N}\mathcal{T}}} P(\mathcal{N}\mathcal{T}^F)}{\prod_{u \in set_k^F} \left(\prod_{r_i \in set_{k,u}^{\mathcal{P}\mathcal{T}}} P(r_i, \mathcal{S}_{i,k,u}^F) \prod_{r_i \in set_{k,u}^{\mathcal{P}\mathcal{F}}} P(\mathcal{F}_{i,k,u}^F) \prod_{r_i \in set_{k,u}^{\mathcal{N}\mathcal{T}}} P(\mathcal{N}\mathcal{T}^F) \right)} \quad (21)$$

where set_k^F is the set of all the available floor indexes in the autonomous block k.

C. Joint Optimization and Final Floor Identification

Our system estimates the final floor with the joint optimization of autonomous blocks and related floors. As equation (22) reveals, $P(F_j, B_k|fp)$ is the joint probability of floor F_j and autonomous block B_k, given an online Wi-Fi scan result fp. set^F and set^B are the sets of all the available floor and autonomous block numbers of the building. The estimated floor number is the one that maximizes the probability of $P(F_j, B_k|fp)$.

$$[F_j, B_k] = \underset{j \in set^F, k \in set^B}{argmax} P(F_j, B_k|fp) \quad (22)$$

As equation (23) shows, the probability $P(F_j, B_k|fp)$ is equal to the product $P(B_k|fp)$ and $P(F_j|fp, B_k)$, which have been calculated in equations (18) and (21).

$$P(F_j, B_k|fp) = \frac{P(F_j|fp, B_k)P(B_k|fp)P(fp)}{P(fp)}$$
$$= P(B_k|fp)P(F_j|fp, B_k) \quad (23)$$

Taking the equation (23) into (22), the equation (22) can be updated as the equation (24).

$$[F_j, B_k] = \underset{j \in set^F, k \in set^B}{argmax} P(B_k|fp)P(F_j|fp, B_k) \quad (24)$$

Taking the equation (18) and (21) into the equation (24), through the equation (25) we estimate the floor on which the user is located.

$$[F_j, B_k] = \underset{j \in set^F, k \in set^B}{argmin} -lgP(B_k|fp) - lgP(F_j|fp, B_k) \quad (25)$$

As a summary, in the offline phase, Wi-Fi fingerprint samples are clustered into autonomous blocks. Then the system evaluates every block and every related floor to construct the autonomous block and local floor detection models. Finally, in the online phase, the system utilizes equation (25) to calculate the joint probability of every autonomous block and the floor probabilities within every block and select the maximum probability prediction as the result.

The time complexity of the system is $O(N^A)$, that is proportional to the number of all the APs detected in the building.
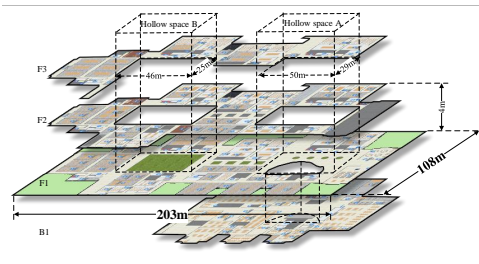
Fig. 9. The floor plan of our experimental training center building.

VI. Implementation and Results Evaluation

A. Experimental Environment

We have conducted our experiments in a large conference centre shown in Fig. 9. The building has four floors and sprawls over an area of $108m \times 203m$. The floor height is $4m$. Three floors are above the ground and one floor is below the ground. The building contains two large hollow spaces and several small courtyards. The size of the two large hollow spaces is 1150 and 1250 m^2 respectively.

We have collected Wi-Fi data of the whole building with two Huawei Mate 9 and a Xiaomi Mix 2 smartphones. We developed a sampling application to collect Wi-Fi fingerprints. A site-surveyor inputted start and end point in the application, then he slowly walked along a line to periodically collect fingerprints. We used one sample line for corridors narrower than 4 meters, and parallel lines for that greater than 4 meters. It takes about half a day to sample the whole building once with a single smartphone. The Mate 9 A collected 6486 samples on July 1st and collected 6517 samples on August 17th. The Mate 9 B collected 6408 samples on August 1st. The Mix 2 only collected 1630 samples on August 2nd, because the sampling frequency of the Mix 2 is about one-fourth of the Mate 9. Each data collection fully covers the four-floor $60,000m^2$ testbed. These data have been collected while users were walking. Based on our survey, 4058 MACs have been detected in this testbed. The number of Wi-Fi stations is about one-third of the total number of MACs, because most of the APs generate three different MAC for different kinds of users, including guests, employees, and administrators. Besides, these APs automatically adjust their broadcasting power every day to optimize the communication capacity, but the adjusting rule is unknown. We also tested our algorithm on a commercial smartphone and the average running time for one request was $160ms$.

B. Cluster Evaluation

The weight coefficient α in equation (2) is a key parameter in clustering fingerprints. This test examines the clustering effect of different weight coefficients. Fig. 10 reveals three typical cases we have examined: clustering with only RSSI similarity ($\alpha = 1$), clustering with only spatial similarity ($\alpha = 0$), clustering with RSSI and spatial similarity ($\alpha = 0.5$). Fig. 10 (a)(c)(e) depict with different colours where the autonomous blocks have been identified on floor 1 (F1). Fig. 10 (b)(d)(f) illustrate the fingerprints of an autonomous block choosing different α value. A comparison between (a) and (c) shows that the RSSI similarity based only on clustering is not able to properly represent the entire building structures.
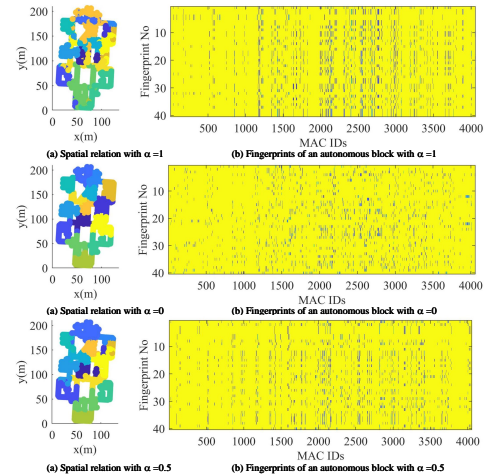

Fig. 10. The similarity of spatial relationships and clustered fingerprints with different weight coefficients.
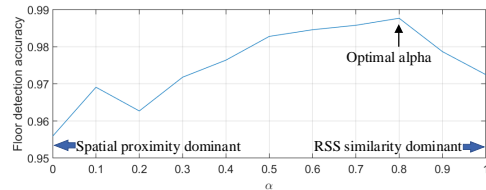

Fig. 11. Floor identification accuracy with different α.

On the other hand, comparing (b) and (d), it can be found that fingerprint consistency is low in (d). Therefore, as (e) and (f) reveal, when both RSSI similarity and spatial proximity are considered, for example, $\alpha = 0.5$, fingerprints within the same autonomous block reveal better consistency both in RSSI and Euclidean spaces.

Fig. 11 shows the influence of different α value in floor identification performances. It can be observed that a proper combination of RSSI similarity or spatial proximity is helpful in improving autonomous block clustering and floor identification accuracy. In this experiment, $\alpha = 0.8$ is the optimal value.

C. Number of Autonomous Blocks

This experiment examines the efficiency of the elbow method in finding the optimal autonomous block number. As Fig. 12 reveals, the floor detection accuracy quickly improves as the number of autonomous blocks increases and reaches the maximum around the elbow point. In other words, a good fingerprint clustering is also a good separation of autonomous blocks. Around the elbow point, Wi-Fi fingerprints of the same autonomous block are more similar. Consequently, by reducing the influence of the fingerprints gathered at faraway places on the same floor, the floor detection accuracy of our model improves. Fig. 13 depicts the autonomous blocks of the testing site. A point in the figure represents a sample. It can be observed that autonomous blocks around hollow areas tend to include multiple floors.

D. Evaluation of Sample Density

The proposed model is based on the Bayesian theory, thus the number of samples directly influences the model efficiency and the floor identification accuracy. Fig. 14 reveals the relationship between floor identification accuracies,
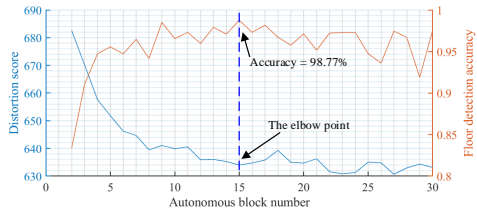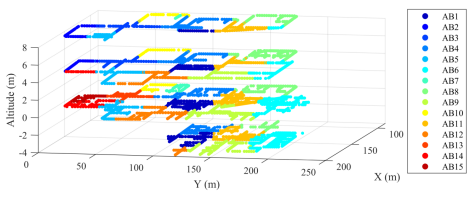
Fig. 12. Setting K with the elbow method.

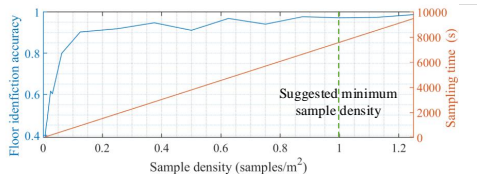Fig. 13. Autonomous blocks of the building.

Fig. 14. Floor identification accuracy of different sample densities.

Fig. 15. Signal strength influence and factor importance analysis.

Fig. 16. Floor identification accuracy comparisons of different algorithms.

sampling time, and average sample density. It can be found that accuracy improves as the sample density increases. When the sample density is greater than 1 $sample/m^2$, the floor identification accuracies become stable. We also estimate the relative minimum sampling time is about 2.5 hours.

E. Evaluation of Signal Strength Related Factors

In order to evaluate the performance of signal strength related factors, we conducted three group of comparisons: under a certain AP and 10 meters away from the AP; slow ($\sim 0.8m/s$) and fast walking ($\sim 2m/s$); workday (less users) and weekend (more users). The result is shown in Fig. 15 (a). It can be found that our system is robust to signal strength variance.

The robustness is a consequence of the features we use in the system. In fact, signal strength mainly influences the performance in atrium areas. As Fig. 15 (b) reveals, we tested the importance of the three level of granularity. The high granularity PN is the probability of $P(\mathcal{NT})$; middle granularity PNF is the joint probability of P($\mathcal{NT}$), P($\mathcal{F}$) and P($\mathcal{S}$), and low granularity is the joint probability of P($\mathcal{NT}$), P($\mathcal{F}$), P($\mathcal{S}$) and the signal strength factor $P(r|\mathcal{S})$. In small or narrow areas, for example a corridor, the improvement of adding signal strength factors is trivial because the distinguishability of negative APs is prominent. Even in wide or atrium areas, higher and middle granularity already reach a decent accuracy and the improvement of signal strength factors are limited. Finally, our system leverages the probability of multiple APs to estimate the results, therefore, even when the signal strength of a single AP varies (because the user approaches or leaves an AP), other AP will ensure the system robustness.

F. Performance Comparison with Different Time/Devices

In order to evaluate the performance of the proposed algorithm, we compare our algorithm with three state-of-the-
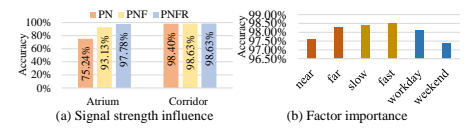
art floor identification methods—HYFI [12], LDA [13], and XGBoost [25]—in the testing of time migration, device heterogeneity, and performance in the hollow area. All methods are trained with the data collected by Mate 9 A on July 1st. Fig. 16 (a) reveals the time migration test. It examines floor detection accuracies with the August 1st data collected by the same Mate 9 A of the training dataset. The result shows that the four algorithm reaches remarkable accuracies. The proposed and XGBoost methods are better than the other two algorithms.
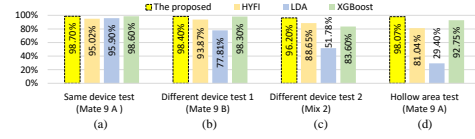
Fig. 16 (b) and (c) show the results of the device heterogeneity test. Due to hardware differences (e.g., antenna gains and different Wi-Fi chips), the received AP RSSI in fingerprints varies for different devices. The (b) is two devices of the same brand and the (c) is of different brands. Although all the performances of the four algorithms drop, our algorithm is more robust than others because the proposed enhanced Bayesian Wi-Fi model fully utilizes the probabilities of $\mathcal{PF}$, $\mathcal{NT}$ and $\mathcal{NF}$ events. The probabilities of these events are more robust than RSSI features used in state-of-the-art algorithms.

Hollow areas, for example, the autonomous block 1 in Fig. 4, are more challenging in floor detection than nonhollow areas because no obstacles are present to attenuate AP signals on different floors. Fig. 16 (d) reveals that the proposed algorithm is more adaptive to complicated buildings with hollow area scenarios. In fact, our algorithm is able to detect the coarse area in which the fingerprints have been collected through an autonomous block clustering. Then, it leverages a suitable local Wi-Fi model to exactly estimate at which floor the user is. For example, the LDA method assumes that all the APs are visible on each floor of the building, thus the method is not suitable to be directly applied in large and multi-storey environments.

G. Evaluation of different devices

We also perform tests on extensive devices based on the UJIIndoorLoc [26] dataset. The selected dataset was collected with 18 different devices in 2 buildings at Universitat Jaume. 15268 samples were collected, 4422 of them are used for training, and 10846 samples for validation. The evaluation results of the four algorithms are shown in TABLE 5. It is worth noting that every device only covers a part of the building and the number of samples collected from the devices is also different. Therefore, the last row of the table also calculates the average accuracy of these devices. Again, the proposed algorithm is more accurate and robust if compared

TABLE V
FLOOR IDENTIFICATION ACCURACY WITH MORE DEVICES

No.	Building 1				Building 2			
	Prop.	HYFI	LDA	XGB	Prop.	HYFI	LDA	XGB
1	100%	100.0%	92.5%	98.7%	98.9%	87.40%	82.0%	98.2%
2	100%	100.0%	97.0%	99.3%	98.2%	81.24%	83.5%	98.2%
3	100%	99.6%	96.6%	100%	93.9%	60.2%	77.1%	86.7%
4	100%	99.6%	84.0%	96.8%	91.4%	75.5%	71.2%	86.1%
5	100%	95.3%	100.0%	100%				
6	100%	95.6%	96.8%	100%	Deveic List			
7	100%	23.4%	91.8%	99.6%			GT-I8160	HTC One
8	98.2%	90.7%	86.7%	97.7%			GT-I9100	LT22i
9	97.2%	51.6%	70.9%	94.8%			GT-S5360	LT26i
10	96.5%	89.5%	95.0%	96.2%			GT-S6500	M1005D
11	96.2%	89.6%	85.4%	97.1%			Galaxy Nexus	Nexus 4
12	95.1%	87.4%	97.1%	99.0%			Orange Monte Carlo	BQ Curie
13	92.3%	84.6%	77.8%	93.2%			Transformer TF101	Celkon A27
14	90.6%	70.3%	79.6%	67.1%			HTC Wildfire S	HTC Desire
15	88.2%	84.2%	80.2%	93.98%				
16	88.1%	98.1%	79.9%	98.98%				
Average	96.4%	84.4%	87.9%	95.8%	95.6%	76.1%	78.5%	92.3%

to the other three algorithms. Performances of the XGBoost algorithm show wide differences in No. 14 building 1 and No. 3 and 4 building 2 because the three devices only appeared in the test dataset. We suppose that the XGBoost algorithm tends to overfit.

VII. CONCLUSION

In large and multi-storey environments, the complexity of Wi-Fi signals on the same floor exceeds the complexity between the floors along the vertical direction, leading to a reduced floor distinguishability. Furthermore, the increasing complexity of Wi-Fi features in complex environments, including atrium/hollow areas, large floor size, and crowded signal channels reduce the performance of Wi-Fi based system for floor identification. Therefore, we propose the adaptive Wi-Fi based floor identification algorithm. Our proposal clusters Wi-Fi fingerprints of a large-scale building into multiple autonomous blocks that have similar RSSI and spatial features. Then, Wi-Fi models are applied to tackle Wi-Fi complexity. We have tested our algorithm with 19 devices, different in types and brands. The experimental results show that our proposal reaches averages accuracies of 97.84%, 96.42%, and 95.67% in three real large buildings.

REFERENCES

[1] F. Potorti, S. Park, A. R. J. Ruiz, P. Barsocchi, M. Girolami, A. Crivello, S. Lee, J. Lim, J. Torressospedra, and F. Seco, "Comparing the performance of indoor localization systems through the evaal framework," *Sensors*, vol. 17, no. 10, p. 2327, 2017.

[2] M. Yang, L. Chuo, K. Suri, L. Liu, H. Zheng, and H. Kim, "ilps: Local positioning system with simultaneous localization and wireless communication," in *IEEE INFOCOM 2019 - IEEE Conference on Computer Communications*, Conference Proceedings, pp. 379–387.

[3] F. Potortì, A. Crivello, M. Girolami, E. Traficante, and P. Barsocchi, "Wi-fi probes as digital crumbs for crowd localisation," in *2016 International Conference on Indoor Positioning and Indoor Navigation (IPIN)*, Conference Proceedings, pp. 1–8.

[4] W. Shao, H. Luo, F. Zhao, H. Tian, S. Yan, and A. Crivello, "Accurate indoor positioning using temporal-spatial constraints based on wi-fi fine time measurements," *IEEE Internet of Things Journal*, pp. 1–1, 2020.

[5] H. S. Maghdid, A. Al-Sherbaz, N. Aljawad, and I. A. Lami, "Unils: Unconstrained indoors localization scheme based on cooperative smartphones networking with onboard inertial, bluetooth and gnss devices," in *Position, Location and Navigation Symposium (PLANS), 2016 IEEE/ION*. CooperativePositioning: IEEE, Conference Proceedings, pp. 129–136.

[6] W. Shao, H. Luo, F. Zhao, C. Wang, A. Crivello, and M. Z. Tunio, "Depedo: Anti periodic negative-step movement pedometer with deep convolutional neural networks," in *2018 IEEE International Conference on Communications (ICC)*, Conference Proceedings, pp. 1–6.

[7] Q. Wang, L. Ye, H. Luo, A. Men, F. Zhao, and C. Ou, "Pedestrian walking distance estimation based on smartphone mode recognition," *Remote Sensing*, vol. 11, no. 9, p. 1140, 2019.

[8] Y. Li, Z. Ghassemlooy, X. Tang, B. Lin, and Y. Zhang, "A vlc smartphone camera based indoor positioning system," *IEEE Photonics Technology Letters*, vol. 30, no. 13, pp. 1171–1174, 2018.

[9] W. Shao, H. Luo, F. Zhao, Y. Ma, Z. Zhao, and A. Crivello, "Indoor positioning based on fingerprint-image and deep learning," *IEEE Access*, pp. 1–1, 2018.

[10] W. Shao, H. Luo, F. Zhao, C. Wang, A. Crivello, and M. Z. Tunio, "Mass-centered weight update scheme for particle filter based indoor pedestrian positioning," in *2018 IEEE Wireless Communications and Networking Conference (WCNC)*, Conference Proceedings, pp. 1–6.

[11] W. Shao, F. Zhao, C. Wang, H. Luo, T. Muhammad Zahid, Q. Wang, and D. Li, "Location fingerprint extraction for magnetic field magnitude based indoor positioning," *Journal of Sensors*, vol. 2016, p. 16, 2016. [Online]. Available: http://dx.doi.org/10.1155/2016/1945695

[12] F. Zhao, H. Luo, X. Zhao, Z. Pang, and H. Park, "Hyfi: Hybrid floor identification based on wireless fingerprinting and barometric pressure," *IEEE Transactions on Industrial Informatics*, vol. 13, no. 1, pp. 330–341, 2017.

[13] J. Luo, Z. Zhang, C. Wang, C. Liu, and D. Xiao, "Indoor multifloor localization method based on wifi fingerprints and lda," *IEEE Transactions on Industrial Informatics*, vol. 15, no. 9, pp. 5225–5234, 2019.

[14] Z.-l. Deng, W. Wang, and L.-m. Xu, "A k-means based method to identify floor in wlan indoor positioning system," *Software*, vol. 33, no. 12, pp. 114–117, 2012.

[15] K. S. Kim, "Hybrid building/floor classification and location coordinates regression using a single-input and multi-output deep neural network for large-scale indoor localization based on wi-fi fingerprinting," in *2018 Sixth International Symposium on Computing and Networking Workshops (CANDARW)*. IEEE, Conference Proceedings, pp. 196–201.

[16] R. Elbakly, M. Elhamshary, and M. Youssef, "Hyrise: A robust and ubiquitous multi-sensor fusion-based floor localization system," *Proceedings of the ACM on Interactive, Mobile, Wearable and Ubiquitous Technologies*, vol. 2, no. 3, pp. 1–23, 2018.

[17] Y. Li, Z. Gao, Z. He, P. Zhang, R. Chen, and N. El-Sheimy, "Multi-sensor multi-floor 3d localization with robust floor detection," *IEEE Access*, vol. 6, pp. 76 689–76 699, 2018.

[18] G. Caso, L. De Nardis, F. Lemic, A. Handziski, A. Wolisz, and M.-G. Di Benedetto, "Vifi: Virtual fingerprinting wifi-based indoor positioning via multi-wall multi-floor propagation model," *IEEE Transactions on Mobile Computing*, 2019.

[19] D. Banerjee, S. K. Agarwal, and P. Sharma, "Improving floor localization accuracy in 3d spaces using barometer," in *Proceedings of the 2015 ACM International Symposium on Wearable Computers*, Conference Proceedings, pp. 171–178.

[20] I. Bisio, A. Sciarrone, L. Bedogni, and L. Bononi, "Wifi meets barometer: Smartphone-based 3d indoor positioning method," in *2018 IEEE International Conference on Communications (ICC)*. IEEE, Conference Proceedings, pp. 1–6.

[21] P. Davidson and R. Piché, "A survey of selected indoor positioning methods for smartphones," *IEEE Communications Surveys & Tutorials*, vol. 19, no. 2, pp. 1347–1370, 2017.

[22] T. Kanungo, D. M. Mount, N. S. Netanyahu, C. D. Piatko, R. Silverman, and A. Y. Wu, "An efficient k-means clustering algorithm: analysis and implementation," *IEEE Transactions on Pattern Analysis and Machine Intelligence*, vol. 24, no. 7, pp. 881–892, 2002.

[23] S. Temma, M. Sugii, and H. Matsuno, "The document similarity index based on the jaccard distance for mail filtering," in *2019 34th International Technical Conference on Circuits/Systems, Computers and Communications (ITC-CSCC)*. IEEE, Conference Proceedings, pp. 1–4.

[24] D. J. Ketchen and C. L. Shook, "The application of cluster analysis in strategic management research: An analysis and critique," *Strategic Management Journal*, vol. 17, no. 6, pp. 441–458, 1996.

[25] J. Huang, H. Luo, W. Shao, F. Zhao, and S. Yan, "Accurate and robust floor positioning in complex indoor environments," *Sensors*, vol. 20, no. 9, p. 2698, 2020.

[26] J. Torres-Sospedra, R. Montoliu, A. Martínez-Usó, J. P. Avariento, T. J. Arnau, M. Benedito-Bordonau, and J. Huerta, "Ujiindoorloc: A new multi-building and multi-floor database for wlan fingerprint-based indoor localization problems," in *2014 International Conference on Indoor Positioning and Indoor Navigation (IPIN)*, Conference Proceedings, pp. 261–270.